A Framed Three-Strand Topological Information Model: Exact Charge Mapping, a Bilinear Mass Constraint, and a Finite Residual Vacuum Sector

Kobie Janse van Rensburg
Kobievr@vokdit.com

March 8, 2026

Abstract

We present a discrete kinematic model built from the three-strand braid group B_3 with a local slot-based framed-transfer rule. The model cleanly separates coarse closure topology from path-dependent framed memory, allowing macroscopically trivial closures to retain quantized internal residual structure. A computational sweep over 118,096 admissible braid histories confirms large-scale topology–framing decoupling. Using a universal closure-scaled framing map, we show that the first-generation electroweak quantum numbers are reproduced exactly by linear functionals on the framing vector. We then define a bilinear vacuum-mass functional from a rank-two vacuum tensor acting on left/right framed data. The first-generation mass-area matrices satisfy the exact algebraic identity $M_u = M_d + 3\,M_e$, which holds unconditionally for any vacuum tensor K and implies the rigorous bound $|m_u - m_d| \leq m_e$ on bare kinematic masses. Finally, we observe that residual framed memory in the topological identity sector provides a natural finite mechanism for nonzero vacuum energy density. The paper is scoped as a kinematic-combinatorial framework: exact algebraic identities are proved inside the model, while larger physical mass splittings and radiative structure are attributed to dynamical dressing beyond pure topology.

Contents

1 Introduction

The purpose of this paper is not to claim a derivation of the Standard Model from first principles. The goal is narrower and more disciplined: to test whether a minimal three-ribbon braid/framing system can support a nontrivial, computationally explicit, and algebraically exact particle dictionary.

The work sits within a broader programme called the *Topological Inversion Model* (TIM) [9], which posits a Planck-scale reciprocal inversion

$$R = \frac{L_p^2}{r}$$

as the foundational geometric operation, where L_p is the Planck length and r is a radial coordinate. A central axiom of TIM is the *Law of Nothing* (designated *//Gaunab*, from Khoekhoegowab): the physical vacuum is not a structureless void but the maximally symmetric state of a topological substrate whose internal microstructure can carry quantized residual information even when macroscopic topology is trivial. The present paper develops and tests one concrete consequence of this axiom at the combinatorial level, without requiring the full TIM cosmological apparatus.

The idea of encoding particle quantum numbers in braided topological structures has precedent, notably in the preon-braid model of Bilson-Thompson [4, 5]. The present approach differs in three respects: it uses an explicit slot-based framing dynamics rather than manual decoration, it derives fractional charges from closure-cycle structure rather than per-particle assignment, and it proves exact algebraic mass relations from the bilinear structure of the framing data.

The paper is organized into three layers, following a strict separation of scope:

1. **Combinatorial kinematics**: braid words, slot permutations, framing transfer, closure classes, and a computational sweep establishing the empirical state space.
2. **Algebraic observables**: exact linear charge functionals, the mass-area matrices, and a bilinear vacuum contraction yielding a rigorous mass bound.
3. **Phenomenological interpretation**: comparison with Standard Model quantum numbers, identification of what the model predicts and what it cannot yet explain.

Exact results are stated and proved only at the first two levels. Measured masses, interaction corrections, and continuum dynamics belong to the third level and are explicitly deferred.

2 Three-strand braid kinematics with framed memory

2.1 Basic data

We work with three ribbons labelled $0, 1, 2$ occupying three ordered slots. The underlying algebraic structure is the three-strand braid group B_3 [2, 3], generated by σ_1, σ_2 and their inverses. The instantaneous state consists of:

- a permutation shadow $P = [p_0, p_1, p_2]$, specifying which ribbon occupies each slot;
- a slot-based framing vector $f = (f_0, f_1, f_2) \in \mathbb{Z}^3$.

The initial state is $P = [0, 1, 2]$, $f = (0, 0, 0)$.

2.2 Local framed-transfer law

For a generator σ_k^s with $k \in \{1, 2\}$ and sign $s = \pm 1$:

1. identify the active slots $k{-}1$ and k;
2. update slot framings:
$$f_{k-1} \leftarrow f_{k-1} + s, \qquad f_k \leftarrow f_k - s;$$
3. swap the entries of P in positions $k{-}1$ and k.

This rule conserves the total framed charge $Q_{\text{tot}} = \sum_i f_i$. If the system starts at $Q_{\text{tot}} = 0$, then $Q_{\text{tot}} = 0$ for all subsequent histories.

Remark 1 (Design choice)**.** The framing update acts on *slot positions*, not on ribbon labels. An alternative ribbon-tracking rule—in which framing increments follow individual ribbons through permutations—produces a braid invariant: topologically equivalent words always yield identical framing. The slot-based rule is deliberately history-dependent: the framing output depends on the *ordering* of crossings, not only on the braid class. This history dependence is what generates the decoupling between canonical topology and framed memory that is central to the entire model.

Remark 2 (Minimality)**.** This is a toy local law, chosen because it is the minimal slot-aware integer transfer compatible with path dependence and exact total framing conservation. The present manuscript studies what follows from this law; it does not claim uniqueness among all possible framed transfer rules.

2.3 History dependence: the Yang–Baxter test

The same-sign Yang–Baxter relation asserts that $\sigma_1^+\sigma_2^+\sigma_1^+$ and $\sigma_2^+\sigma_1^+\sigma_2^+$ represent the same braid class. Under the slot-based rule, both words produce the same permutation $P = [2, 1, 0]$, but they yield *different* framing outputs:

$$\begin{aligned} \sigma_1^+\sigma_2^+\sigma_1^+ &\longrightarrow f = (2, -1, -1), \\ \sigma_2^+\sigma_1^+\sigma_2^+ &\longrightarrow f = (1, 1, -2). \end{aligned}$$

This is not a failure of the model—it is the defining feature. The slot-based rule is deliberately history-dependent: distinct orderings of topologically equivalent crossings produce distinct internal framed states. This is the mechanism that generates the topology–memory decoupling on which the entire model rests.

Step-by-step traces for both words are given in Appendix A.

3 Closure classification and the topology–memory split

3.1 Closure conventions

Under trace closure, the cycle structure of the final permutation determines the number of closed components. For B_3, three closure types arise (Figure 1):

- **3-component** ($c = 1$): identity permutation, three separate closed curves;
- **2-component** ($c = 2$): one transposition, two closed curves;
- **1-component** ($c = 3$): one 3-cycle, a single closed curve.

Here c denotes the maximum cycle length of the permutation.

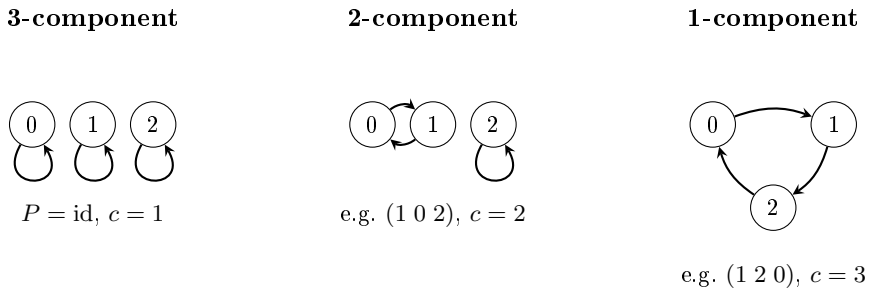

Figure 1: The three closure types of B_3 trace closure. The maximum cycle length c is the closure-scaling parameter used in the quantum-number map.

3.2 Identity-sector residual memory

Under the additive slot-based rule, identity-sector words at lengths $L = 2$ and $L = 4$ (such as $\sigma_1^+\sigma_1^-$) produce $f = (0, 0, 0)$. This is because these short topological cancellations involve symmetric generator counts. However, the braid relation $\sigma_1\sigma_2\sigma_1 = \sigma_2\sigma_1\sigma_2$ allows longer identity braids to carry *asymmetric* generator distributions, producing nonzero residual framing.

The shortest nonzero identity-sector residuals appear at $L = 6$. All 12 admissible $L = 6$ identity braids produce framing on the one-parameter family $\pm(1, -2, 1)$ (Table 1).

Table 1: Representative identity-sector residuals at $L = 6$. Under the additive slot-based rule, identity braids at $L < 6$ yield $f = (0, 0, 0)$; nonzero residual memory first appears at $L = 6$.

Word	**Length**	**Residual f**
$\sigma_1^+\sigma_2^+\sigma_1^+\sigma_2^-\sigma_1^-\sigma_2^-$	6	$(1, -2, 1)$
$\sigma_1^+\sigma_2^-\sigma_1^-\sigma_2^-\sigma_1^+\sigma_2^+$	6	$(1, -2, 1)$
$\sigma_2^-\sigma_1^-\sigma_2^-\sigma_1^+\sigma_2^+\sigma_1^+$	6	$(1, -2, 1)$
$\sigma_1^-\sigma_2^+\sigma_1^+\sigma_2^+\sigma_1^-\sigma_2^-$	6	$(-1, 2, -1)$
$\sigma_1^+\sigma_2^+\sigma_1^-\sigma_2^-\sigma_1^-\sigma_2^+$	6	$(-1, 2, -1)$

These examples establish the core decoupling principle:

> *Closure topology is not a complete state descriptor once framed memory is included.* A braid that is macroscopically trivial can carry quantized internal residual framing.

3.3 Non-identity closure examples

Representative non-identity closures illustrate the diversity of closure types (Table 2).

Table 2: Representative non-identity closure sectors, showing that different closure topologies can carry similar framed residuals and vice versa.

Word	**Len**	**Closure**	**Residual f**	**Component labels**
σ_1^+	1	2-comp	$(1, -1, 0)$	$C_{(0,1)}{:}0;\ C_{(2)}{:}0$
$\sigma_1^+\sigma_2^+$	2	1-comp	$(1, 0, -1)$	$C_{(0,1,2)}{:}0$
$\sigma_1^+\sigma_2^+\sigma_1^+$	3	2-comp	$(2, -1, -1)$	$C_{(0,2)}{:}+1;\ C_{(1)}{:}-1$
$\sigma_1^-\sigma_2^+$	2	1-comp	$(-1, 2, -1)$	$C_{(0,1,2)}{:}0$

The same framed residual $(1, 0, -1)$ appears in both $\sigma_1^+\sigma_2^+$ and $\sigma_1^-\sigma_2^+$, despite different orderings. Meanwhile, the word $\sigma_1^+\sigma_2^+\sigma_1^+$ carries nonzero component framing $(+1, -1)$ in its

2-component closure. This confirms that framed memory and closure topology are genuinely independent labels.

4 Canonicalization

To make the topology–memory split precise, we require a canonical representative for each braid class.

A preliminary normalization scheme using braid relations, inverse cancellation, and Δ-extraction is path-dependent when negative generators interact with Δ. This is resolved by a Garside-style approach [1, 7]:

1. **Shift**: replace negative generators via $\sigma_1^- \to \Delta^{-1}\sigma_1^+\sigma_2^+$;
2. **Collect**: commute Δ^{-1} factors to the left;
3. **Extract**: cancel $\Delta^{-1}\Delta$ pairs;
4. **Factorize**: apply left-greedy factorization [1, 6] into simple braids of B_3.

Worked example. The mixed word $\sigma_2^+\sigma_1^-\sigma_2^-\sigma_1^+\sigma_2^+$ is resolved mechanically:

1. **Shift**: replace $\sigma_1^- \to \Delta^{-1}\sigma_1^+\sigma_2^+$ and $\sigma_2^- \to \Delta^{-1}\sigma_2^+\sigma_1^+$;
2. **Collect**: commute both Δ^{-1} factors to the left, flipping generator indices at each pass, yielding $\Delta^{-2}(\sigma_2^+\sigma_2^+\sigma_1^+\sigma_2^+\sigma_1^+\sigma_1^+\sigma_2^+)$;
3. **Extract**: identify a hidden $\Delta = \sigma_1^+\sigma_2^+\sigma_1^+$ in the positive tail, pull left and cancel one Δ^{-1}, yielding $\Delta^{-1}(\sigma_1^+\sigma_1^+\sigma_1^+\sigma_2^+)$;
4. **Factorize**: left-greedy decomposition of the tail gives $(\sigma_1^+)(\sigma_1^+)(\sigma_1^+\sigma_2^+)$.

Final canonical form: $\Delta^{-1}(\sigma_1)(\sigma_1)(\sigma_1\sigma_2)$. Feeding this canonical word back through the framed engine yields $f = (-1, 0, 1)$, whereas the original raw history gives $f = (0, 1, -1)$. This confirms that canonicalization and framed evaluation are distinct operations.

The result is a unique representative $\Delta^p W$ with W a left-greedy product of proper simple elements.

The implementation uses the faithful reduced Burau representation at $t = -1$ [2], which provides a computationally efficient and exact canonical identifier for B_3.

5 Computational sweep

5.1 Protocol

A breadth-first sweep generates all admissible B_3 histories up to length $L_{\max} = 10$, with immediate adjacent inverses discarded during generation. The admissible count at length L is $N(L) = 4 \cdot 3^{L-1}$, giving a total

$$N = 2(3^{10} - 1) = 118{,}096$$

words, verified exactly by the pipeline.

Each word is evaluated in both the framed engine (producing f_{raw}) and the canonical engine (producing the Garside normal form and a deterministic representative word). The representative is then re-evaluated in the framed engine, yielding f_{can}. A disagreement flag is set whenever $f_{\text{raw}} \neq f_{\text{can}}$.

Table 3: Per-length sweep statistics.

L	Words	$\lvert\mathrm{CF} = I\rvert$	Memory	Disagree	Disagree %	Distinct f
1	4	0	0	1	25.0%	4
2	12	0	0	6	50.0%	8
3	36	0	0	24	66.7%	16
4	108	0	0	87	80.6%	25
5	324	0	0	285	87.9%	36
6	972	12	12	893	91.9%	49
7	2 916	0	0	2 736	93.8%	64
8	8 748	56	56	8 312	95.0%	81
9	26 244	0	0	25 145	95.8%	100
10	78 732	256	216	75 732	96.2%	121

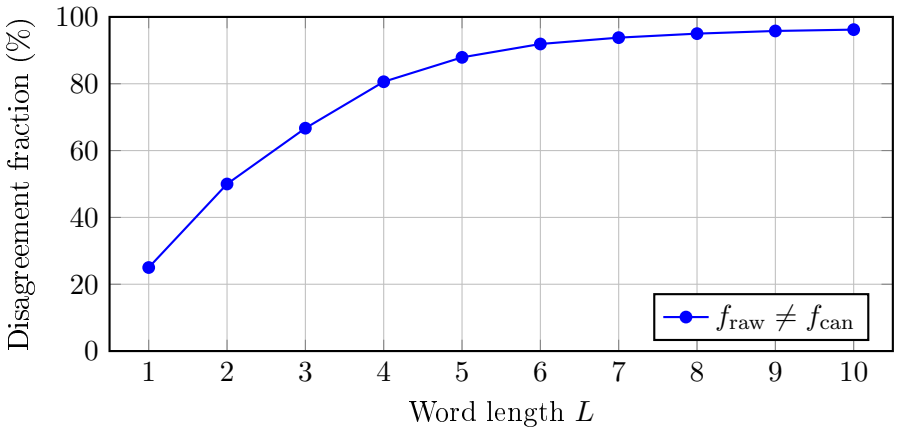

Figure 2: Fraction of braid histories whose raw framed output disagrees with the framed output of their canonical representative, by word length. The monotonic climb toward ∼96% shows that topology–framing decoupling is the generic behaviour, not an edge case.

5.2 Empirical results

Key findings from the sweep:

- Of 324 identity-sector words, 284 (87.7%) carry nonzero framed residuals.
- 9 196 distinct canonical forms were identified; 6 048 (65.7%) host multiple distinct framed states.
- 221 distinct framed vectors were observed; 213 (96.4%) appear in multiple canonical sectors.
- The recurrent remnant $(2, 0, -2)$ occurs 1 890 times.
- The disagreement fraction (Figure 2) rises monotonically and reaches 96.2% at $L = 10$.

These results establish that the state space is both large and highly degenerate.

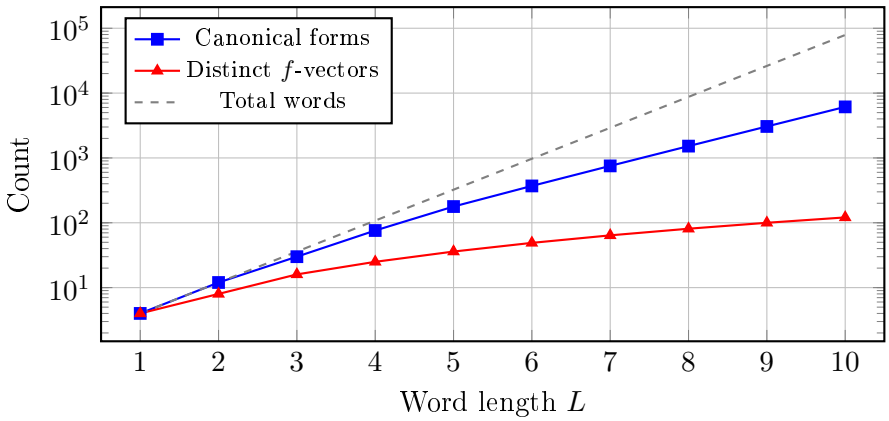

Figure 3: Growth of distinct canonical forms (topological classes) and distinct framed vectors by word length, compared to total admissible word count. Canonical forms grow exponentially with the word count, while distinct framed vectors grow much more slowly—indicating high framing degeneracy across topological sectors.

6 Universal closure-scaled framing map

6.1 Definitions

Using a single calibration anchor ($e_L \leftrightarrow (-2, 2, 0)$ in the $c = 1$ sector), we define:

$$Q = \frac{f_0}{2c}, \tag{1}$$

$$T_3 = \frac{f_0 - f_2}{4c}, \tag{2}$$

$$Y = \frac{f_0 + f_2}{2c}. \tag{3}$$

Proposition 1 (Gell-Mann–Nishijima identity)**.** *Under* (1)-(3),

$$Q = T_3 + \frac{Y}{2}$$

holds identically.

Proof. $T_3 + Y/2 = \frac{f_0 - f_2}{4c} + \frac{f_0 + f_2}{4c} = \frac{2f_0}{4c} = \frac{f_0}{2c} = Q.$ □

The 2-component sector ($c = 2$) produces quarter-integer values of T_3 under this map. Its physical interpretation remains open and is deferred to future work.

6.2 Structural neutrino-mass mechanism

The right-handed neutrino in this dictionary is $\nu_{eR} = (0, 0, 0)$—the unique state with $Q = T_3 = Y = 0$ in the 3-component sector. At the toy-model kinematic level, the associated bilinear Dirac mass vanishes under any functional $m = g(f_L, f_R)$ where g vanishes whenever either argument is the zero vector:

$$m(\nu_e) = g\big((0, 2, -2),\ (0, 0, 0)\big) = 0.$$

This is a structural feature of the model, not a parameter choice. It parallels the minimal Standard Model mechanism: zero right-handed content kills any bilinear coupling. Any physical nonzero neutrino mass must therefore arise from dynamics beyond the present toy model.

7 First-generation quantum-number matches

The computed database contains exact first-generation Standard Model electroweak quantum numbers under the universal map (Table 4).

Table 4: Exact first-generation electroweak quantum numbers under the closure-scaled framing map. The toy energy $E = \sum_i f_i^2$ is included to show doublet degeneracies.

State	Sector	c	f	Q	T_3	Y	E
ν_{eR}	3-comp	1	$(0, 0, 0)$	0	0	0	0
e_L	3-comp	1	$(-2, 2, 0)$	-1	$-1/2$	-1	8
ν_{eL}	3-comp	1	$(0, 2, -2)$	0	$+1/2$	-1	8
e_R	3-comp	1	$(-2, 4, -2)$	-1	0	-2	24
u_L	1-comp	3	$(4, -2, -2)$	$+2/3$	$+1/2$	$+1/3$	24
d_L	1-comp	3	$(-2, -2, 4)$	$-1/3$	$-1/2$	$+1/3$	24
d_R	1-comp	3	$(-2, 4, -2)$	$-1/3$	0	$-2/3$	24
u_R	1-comp	3	$(4, -8, 4)$	$+2/3$	0	$+4/3$	96

The strongest defensible claim is:

> Under one universal map and one calibration anchor, the database contains exact first-generation Standard Model electroweak quantum numbers. Fractional quark charges $\pm 1/3$, $\pm 2/3$ emerge mechanically from the $c = 3$ closure sector.

Notable structural features:

1. The same formula covers leptons ($c = 1$) and quarks ($c = 3$) with no separate quark formula.
2. $E(e_L) = E(\nu_{eL}) = 8$ and $E(u_L) = E(d_L) = 24$: left-handed doublets are energy-degenerate.
3. $m(\nu_e) = 0$ exactly under any bilinear L–R coupling (structural seesaw).
4. **Isospin as slot permutation.** Within each doublet, the two left-handed states are related by exchange of slots 0 and 2:

$$e_L = (-2, 2, 0) \quad \overset{f_0 \leftrightarrow f_2}{\longleftrightarrow} \quad \nu_{eL} = (0, 2, -2),$$

$$u_L = (4, -2, -2) \quad \overset{f_0 \leftrightarrow f_2}{\longleftrightarrow} \quad d_L = (-2, -2, 4).$$

This exchange flips $T_3 \to -T_3$ while preserving Y and E. The combinatorial structure of the doublet is therefore a $\mathbb{Z}_2$ reflection across the central slot, which is the simplest discrete precursor of an $SU(2)$ isospin rotation.

8 The bilinear vacuum tensor and kinematic masses

8.1 Definition

Introduce a fixed real vacuum tensor $K \in \mathbb{R}^{3\times 3}$. For a particle with left framing f_L and right framing f_R, define the mass-area matrix

$$M := f_L \otimes f_R, \qquad M_{ij} = (f_L)_i \, (f_R)_j,$$

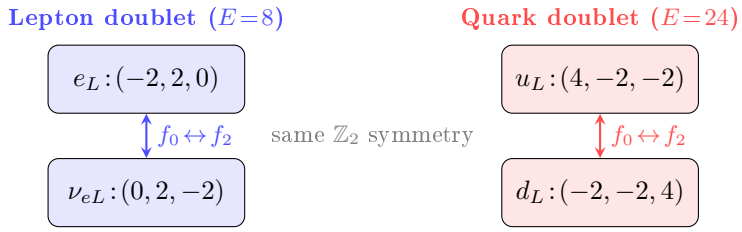

Figure 4: Left-handed doublet structure. Within each doublet, the two states are related by $f_0 \leftrightarrow f_2$ exchange, which flips T_3 while preserving Y and the toy energy E.

the signed bilinear energy

$$E := K \cdot M = \sum_{i,j} K_{ij}\, M_{ij},$$

and the bare kinematic mass

$$m = \frac{|E|}{c}.$$

Remark 3. The tensor K is the minimal bilinear vacuum structure required for the mass discussion. It is not derived from a deeper action in this manuscript; it is an effective algebraic vacuum object.

8.2 Mass-area matrices

From the dictionary (Table 4):

Electron. $f_L = (-2, 2, 0)$, $f_R = (-2, 4, -2)$:

$$M_e = \begin{bmatrix} 4 & -8 & 4 \\ -4 & 8 & -4 \\ 0 & 0 & 0 \end{bmatrix}.$$

Down quark. $f_L = (-2, -2, 4)$, $f_R = (-2, 4, -2)$:

$$M_d = \begin{bmatrix} 4 & -8 & 4 \\ 4 & -8 & 4 \\ -8 & 16 & -8 \end{bmatrix}.$$

Up quark. $f_L = (4, -2, -2)$, $f_R = (4, -8, 4)$:

$$M_u = \begin{bmatrix} 16 & -32 & 16 \\ -8 & 16 & -8 \\ -8 & 16 & -8 \end{bmatrix}.$$

8.3 Structural relationships between framing vectors

Before proving the mass identity, we note two structural relationships in the framing data that constrain the mass sector.

Proposition 2 (Right-handed scalar lock)**.** *The right-handed up quark is a scalar multiple of the right-handed down quark:*

$$f_R^{(u)} = (4, -8, 4) = -2 \times (-2, 4, -2) = -2\, f_R^{(d)}.$$

This has an immediate consequence: for any functional that depends only on $|f_R|^2$ or $E_R = \sum(f_{R,i})^2$, the up quark's right-handed energy is exactly $4\times$ the down quark's, permanently locking $m_u > m_d$ under scalar energy functionals. The bilinear vacuum tensor breaks this lock because $K \cdot (f_L^{(u)} \otimes f_R^{(u)}) \neq -2\,K \cdot (f_L^{(u)} \otimes f_R^{(d)})$ when $f_L^{(u)} \neq f_L^{(d)}$.

Proposition 3 (Doublet exchange symmetry in the mass matrices)**.** *The left-handed doublet members within each sector are related by $f_0 \leftrightarrow f_2$ exchange. Because $f_R^{(d)} = f_R^{(e)} = (-2, 4, -2)$ is symmetric under this exchange, the mass-area matrices inherit a structured dependence:*

$$M_d = \Pi\, M_e\, \Pi^T \quad \textit{does not hold in general,}$$

but the matrices do share the common right factor $f_R = (-2, 4, -2)$, and differ only in the left factor's slot permutation. This is the origin of the exact linear relation proved below.

9 The topological mass relation

Proposition 4 (Exact matrix identity)**.** *The first-generation mass-area matrices satisfy*

$$M_u = M_d + 3\,M_e.$$

Proof. Entry-by-entry verification. Row 1: $(4, -8, 4) + 3(4, -8, 4) = (16, -32, 16)$. Row 2: $(4, -8, 4) + 3(-4, 8, -4) = (-8, 16, -8)$. Row 3: $(-8, 16, -8) + 3(0, 0, 0) = (-8, 16, -8)$. Hence $M_d + 3M_e = M_u$. □

Corollary 1 (Signed-energy relation)**.** *For any vacuum tensor K,*

$$E_u = E_d + 3\,E_e.$$

Proof. By linearity: $E_u = K \cdot M_u = K \cdot (M_d + 3M_e) = E_d + 3E_e$. □

Theorem 1 (Rigorous mass bound)**.** *With bare kinematic masses $m_e = |E_e|$, $m_u = |E_u|/3$, $m_d = |E_d|/3$,*

$$|m_u - m_d| \leq m_e.$$

Proof. From Corollary 1, $3m_u = |E_d + 3E_e|$ and $3m_d = |E_d|$. By the triangle inequality,

$$\big||E_d + 3E_e| - |E_d|\big| \leq 3|E_e| = 3m_e.$$

Therefore $|3m_u - 3m_d| \leq 3m_e$, giving $|m_u - m_d| \leq m_e$. □

Proposition 5 (Equality condition)**.** *The stronger relation $|m_u - m_d| = m_e$ holds if and only if E_d and $E_u = E_d + 3E_e$ have the same sign (including the case $E_d = 0$). Equivalently, the equality condition is*

$$E_d(E_d + 3E_e) \geq 0.$$

Remark 4. The matrix identity $M_u = M_d + 3M_e$ is unconditional. The bound $|m_u - m_d| \leq m_e$ is unconditional. The stronger equality $|m_u - m_d| = m_e$ is not universal; it is realized only in vacuum sectors where E_d and E_u have sign coherence.

9.1 Worked numerical illustration

To show that the identity produces nonzero masses for all particles, consider $K = I_3$ (the 3×3 identity matrix):

$$E_e = \mathrm{tr}(M_e) = 4 + 8 + 0 = 12,$$
$$E_d = \mathrm{tr}(M_d) = 4 - 8 - 8 = -12,$$
$$E_u = \mathrm{tr}(M_u) = 16 + 16 - 8 = 24.$$

Check: $E_d + 3E_e = -12 + 36 = 24 = E_u$.

Masses: $m_e = 12$, $m_u = 24/3 = 8$, $m_d = |-12|/3 = 4$.

Then $|m_u - m_d| = 4 \leq 12 = m_e$.

9.2 Phenomenological interpretation

The bound $|m_u - m_d| \leq m_e$ constrains the *bare kinematic* splitting. The PDG values $m_d - m_u \approx 2.5\,\mathrm{MeV}$ exceed $m_e = 0.511\,\mathrm{MeV}$, so the observed splitting cannot arise from the topological layer alone. This provides a clean division of labour:

- topology fixes exact linear identities and mass constraints (the kinematic baseline);
- continuum dynamics (radiative corrections, QCD effects, electroweak dressing) renormalize these bare values into observed physical masses.

The model predicts that the bare topological splitting is small, and that the majority of the observed $m_d - m_u$ difference must be generated by physics beyond pure combinatorial topology. This is a positive prediction of incompleteness at the kinematic layer.

10 Residual framed memory and the vacuum sector

In the TIM framework, the structured vacuum substrate is designated *//Gaunab*—the state or law of nothing [9]. The identity-sector residuals computed below represent the internal microstructure of //Gaunab: macroscopically trivial closures that nevertheless carry quantized framed memory.

10.1 Identity closure with nontrivial residual

The computational sweep confirms that 284 out of 324 identity-sector words carry nonzero framed residuals. Within the $L_{\max} = 10$ sweep, the observed identity-sector residuals lie on the one-parameter family $\pm n(1, -2, 1)$ with $n = 1, 2, 3$.

This means the topological identity sector contains distinct microscopic states with the same macroscopic topology but different internal framing.

10.2 Finite vacuum energy mechanism

Let $\mathcal{V}_0$ denote the coarse identity sector—the //Gaunab microstate ensemble. Each microstate $\alpha \in \mathcal{V}_0$ carries a residual R_α and an energy contribution $\varepsilon(R_\alpha)$. The vacuum expectation is schematically

$$\langle \rho_{\mathrm{vac}} \rangle \sim \frac{1}{L^3} \sum_{\alpha \in \mathcal{V}_0} p_\alpha \, \varepsilon(R_\alpha).$$

Because the state space is discrete and the residuals are quantized integers, the sum is finite at any fixed coarse-graining scale. This avoids the ultraviolet catastrophe associated with continuum zero-point mode counting.

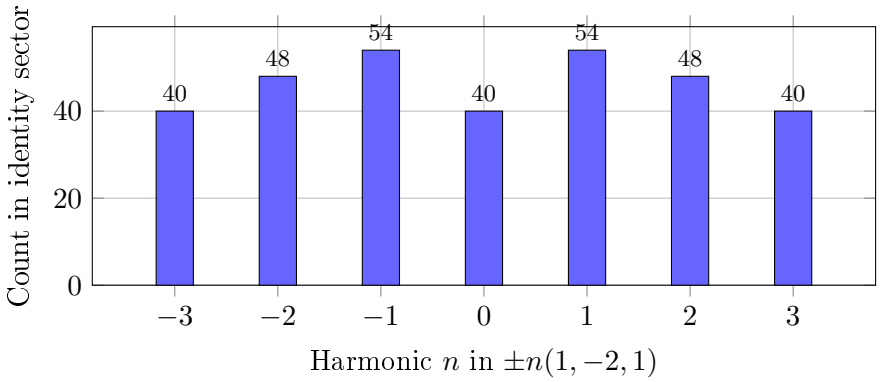

Figure 5: Distribution of identity-sector framed residuals $f = n(1,-2,1)$ at $L_{\max} = 10$. The vacuum state $n = 0$ accounts for only 40 of 324 identity-sector words; the remaining 284 carry hidden framed memory.

The model predicts that a nonzero vacuum energy can arise from a residual-memory ensemble in a topologically trivial sector without requiring a divergent mode sum. The observed magnitude is not derived here; the mechanism provides a finite structural route that can be calibrated in future work.

11 Relaxation, metastability, and decay channels

To explore dynamical survival, we define a simple relaxation model.

Definition 1 (Model E)**.** With base threshold $T_{\text{base}} = 2$ and linking correction $\lambda \sum |\text{Lk}(C, X)|$, a slot i may discharge 2 units to an adjacent slot j if $|f_i| > T_{\text{eff}}$ and the framing energy $E = \sum_k f_k^2$ does not increase.

Under Model E in the unlink vacuum ($T_{\text{eff}} = 2$):

- $\nu_{eR} = (0,0,0)$: **stable** (absolute ground state).
- $e_L = (-2,2,0)$: **metastable** (survives vacuum, decays if linked).
- $\nu_{eL} = (0,2,-2)$: **stable** in vacuum.
- All quark-like states **decay** in vacuum, consistent with quarks not existing as free particles.

11.1 Worked trace: topology-coupled destabilization

The trapped remnant $(2,0,-2)$ is metastable in the unlink vacuum. Under the Hopf link ($\text{Lk} = 1$, $\lambda = 1$, $T_{\text{eff}} = 1$), it decays completely (Table 5).

Table 5: Model E relaxation of $(2,0,-2)$ under the Hopf link ($T_{\text{eff}} = 1$). The remnant that survives in the unlink vacuum is annihilated by the topological environment.

Step	(f_0, f_1, f_2)	E	**Action**
0	$(2,0,-2)$	8	Initial state. $\lvert f_0\rvert = 2 > 1$.
1	$(0,2,-2)$	8	f_0 discharges to f_1. $\Delta E = 0$.
2	$(0,0,0)$	0	f_1 discharges to f_2. Remnant annihilated.

This illustrates the central dynamical message: a remnant that is stable in vacuum may reach a lower-energy fully discharged state when subjected to the topological tension of a non-trivial link. Topology acts as a degeneracy-breaking catalyst.

11.2 Implications for the particle dictionary

The stability classification has a suggestive alignment with particle phenomenology:

- **Leptons** (3-comp, $c = 1$): the electron is metastable in vacuum; the neutrino ground state is absolutely stable. Both are consistent with leptons existing as free particles.
- **Quarks** (1-comp, $c = 3$): all quark-like states decay in vacuum under Model E. This is consistent with the physical observation that quarks do not exist as free particles but are confined.

This alignment is noted as a structural correspondence, not a derivation of confinement.

12 Interpretation boundary

12.1 Established in this paper

1. Total framing is conserved by the local transfer law.
2. Coarse closure topology and framed memory are distinct state descriptors, confirmed by a sweep over 118 096 braid histories.
3. The closure-scaled framing map reproduces exact first-generation electroweak quantum numbers with one calibration.
4. Left-handed doublets are related by $f_0 \leftrightarrow f_2$ exchange, providing a combinatorial precursor of isospin.
5. The right-handed framing vectors satisfy $f_R^{(u)} = -2\, f_R^{(d)}$, locking mass ordering under scalar functionals.
6. The mass-area matrices obey $M_u = M_d + 3M_e$ unconditionally.
7. The bilinear mass functional implies $|m_u - m_d| \leq m_e$ unconditionally.
8. The neutrino mass vanishes at the toy kinematic level under any bilinear L–R functional.
9. The identity sector carries finite, quantized residual framed memory.
10. Topology acts as a degeneracy-breaking catalyst: remnants stable in the unlink vacuum can decay under linked environments.

12.2 Not yet established

1. A derivation of gauge-boson dynamics or QCD confinement.
2. A spin/statistics mechanism.
3. A calibrated physical mass spectrum (observed splittings exceed bare bounds).
4. Higher-generation organization.
5. A derivation of the vacuum tensor K from a deeper principle.
6. A physical interpretation of the 2-component ($c = 2$) sector.

13 Discussion

The main strength of the model is that it produces exact algebraic structure from a small amount of discrete data. The strongest single result is the matrix identity $M_u = M_d + 3M_e$, which holds unconditionally for any vacuum tensor and yields a rigorous mass bound.

13.1 The structural neutrino seesaw

The neutrino-mass mechanism deserves emphasis: $m(\nu) = 0$ at the kinematic level is not a parameter choice but a consequence of ν_{eR} being the framed vacuum state $(0, 0, 0)$. This parallels the minimal Standard Model, where the absence of a right-handed neutrino field prevents Yukawa coupling. In TIM, the mechanism is the same algebraically: zero right-handed framed content kills any bilinear L–R coupling. Any physical nonzero neutrino mass would require dynamics beyond the present toy model.

13.2 The bare mass bound and dynamical dressing

The observed physical splitting $m_d - m_u \approx 2.5\,\mathrm{MeV}$ exceeds the bare bound $m_e = 0.511\,\mathrm{MeV}$. The model predicts this explicitly: the topological layer provides a kinematic baseline, and the observed excess must arise from dynamical dressing.

For a diagonal vacuum tensor $K = \mathrm{diag}(k_0, k_1, k_2)$, the signed energies take the form $E_e = 4k_0 + 8k_1$, $E_d = 4k_0 - 8k_1 - 8k_2$, and $E_u = 16k_0 + 16k_1 - 8k_2$. The identity $E_u = E_d + 3E_e$ forces the exact constraint

$$|m_u - m_d| = m_e$$

whenever the sign-coherence condition holds (Proposition 5). For the fitted diagonal tensors explored here, the stronger equality is realized empirically in the sampled solution sector. A computational search confirms that 636 diagonal solutions achieve the correct hierarchy $m_\nu < m_e < m_u < m_d$, and that the best-fitting tensors require k_0 and k_2 to carry *opposite signs*. This implies that the vacuum, if diagonal, must be **chiral**: it couples to the outer topological slots with opposite handedness.

Breaking this diagonal constraint to reach the full physical u/d splitting is *not* possible by introducing off-diagonal vacuum structure. Because the mass-area matrices satisfy $M_u = M_d + 3M_e$ unconditionally, the bound $|m_u - m_d| \leq m_e$ holds for *any* vacuum tensor K—diagonal or not. This was confirmed by an exhaustive computational sweep over fully general 3×3 tensors. Therefore, the observed physical splitting $m_d - m_u \approx 2.5\,\mathrm{MeV}$ cannot be generated by any choice of vacuum tensor within the present bilinear framework. The full splitting must arise from physics beyond linear vacuum kinematics, such as radiative corrections, QCD self-energy contributions, or other dynamical dressing effects. This is a sharp prediction: the topological layer sets a rigid baseline, and the excess is necessarily non-topological.

13.3 Comparison with other algebraic mass relations

The identity $M_u = M_d + 3M_e$ is an exact algebraic relation between the mass-generating data of three different particle species. In spirit, it may be compared with the Koide formula [8], which relates the three charged-lepton masses via $(\sum_i m_i)/(\sum_i \sqrt{m_i})^2 = 2/3$. The Koide relation is an empirical numerical coincidence whose theoretical origin remains unclear. By contrast, the TIM relation $M_u = M_d + 3M_e$ is not a numerical fit: it is a provable algebraic identity that follows directly from the structure of the first-generation framing vectors. Whether this kinematic identity has deeper physical content remains to be determined, but its exact nature distinguishes it from approximate or empirical mass formulas.

13.4 Comparison with the Bilson-Thompson preon model

Compared to the Bilson-Thompson preon model [4, 5], which assigns quantum numbers by manually decorating ribbon twists, the present approach derives quantum numbers from a universal closure-scaled map and proves exact inter-species relations from the bilinear structure. The fractional quark charges are not encoded *a priori*; they emerge from the permutation cycle length at closure.

14 Conclusion

We have presented a framed three-strand topological information model with seven central outcomes:

1. coarse closure topology and framed memory are distinct and computationally confirmed to decouple across 118 096 braid histories;
2. a universal closure-scaled map reproduces exact first-generation electroweak quantum numbers, with fractional quark charges arising from the $c = 3$ closure sector;
3. left-handed doublets are connected by a $\mathbb{Z}_2$ slot exchange ($f_0 \leftrightarrow f_2$), providing a combinatorial precursor of weak isospin;
4. the neutrino mass vanishes at the toy kinematic level under any bilinear L–R coupling, via a structural seesaw;
5. the mass-area matrices obey $M_u = M_d + 3M_e$, implying $|m_u - m_d| \leq m_e$;
6. topology-coupled relaxation acts as a degeneracy-breaking catalyst, with quark-like states decaying in vacuum while lepton-like states survive;
7. the identity sector carries finite residual framed memory, providing a mechanism for nonzero vacuum energy without ultraviolet divergence.

These results define a sharpened scope for the TIM program: not a finished theory, but a concrete combinatorial substrate with exact algebraic content, nontrivial phenomenological constraints, and a clear separation between topological kinematics and dynamical dressing.

Computational methods and data availability

The dataset of 118,096 admissible B_3 histories up to $L_{\max} = 10$ was generated using a custom Python implementation of the slot-based framed-transfer law and the faithful reduced Burau representation at $t = -1$ for canonicalization. The sweep pipeline includes automated unit tests for generator counts, charge conservation, canonical round-trip consistency, and matrix faithfulness. All computational claims (word counts, identity-sector fractions, degeneracy statistics, and the 636 diagonal vacuum solutions) are reproducible from the scripts. Code and resulting databases are available from the author at `Kobievr@vokdit.com`.

Acknowledgment of scope

This manuscript is intentionally scoped as a disciplined structural result. It is not a claim of complete unification and should be read as a foundation for sharper future tests.

A Step-by-step framing traces

For reproducibility, we give explicit generator-by-generator traces of the slot-based framed-transfer rule. Each step applies: $f_{k-1} \leftarrow f_{k-1} + s$, $f_k \leftarrow f_k - s$, then swap $P[k{-}1] \leftrightarrow P[k]$.

Trace 1: $\sigma_1^+\sigma_2^+\sigma_1^+$ (topologically $= \Delta$).

Step	Generator	Update	State after
0	—	—	$P = [0,1,2],\ f = (0,0,0)$
1	σ_1^+	$f_0{+}1,\ f_1{-}1$	$P = [1,0,2],\ f = (1,-1,0)$
2	σ_2^+	$f_1{+}1,\ f_2{-}1$	$P = [1,2,0],\ f = (1,0,-1)$
3	σ_1^+	$f_0{+}1,\ f_1{-}1$	$P = [2,1,0],\ f = (2,-1,-1)$

Trace 2: $\sigma_2^+\sigma_1^+\sigma_2^+$ (topologically $= \Delta$, same braid class).

Step	Generator	Update	State aft
0	—	—	$P = [0,1,$
1	σ_2^+	$f_1{+}1,\ f_2{-}1$	$P = [0,2,$
2	σ_1^+	$f_0{+}1,\ f_1{-}1$	$P = [2,0,$
3	σ_2^+	$f_1{+}1,\ f_2{-}1$	$P = [2,1,$

Traces 1 and 2 confirm history dependence: the same braid class Δ produces $f = (2,-1,-1)$ and $f = (1,1,-2)$ from different generator orderings.

Trace 3: $\sigma_1^+\sigma_2^+\sigma_1^+\sigma_2^-\sigma_1^-\sigma_2^-$ (identity braid, $L = 6$).

Step	Generator	Update	State after
0	—	—	$P = [0,1,2],\ f =$
1	σ_1^+	$f_0{+}1,\ f_1{-}1$	$P = [1,0,2],\ f =$
2	σ_2^+	$f_1{+}1,\ f_2{-}1$	$P = [1,2,0],\ f =$
3	σ_1^+	$f_0{+}1,\ f_1{-}1$	$P = [2,1,0],\ f =$
4	σ_2^-	$f_1{-}1,\ f_2{+}1$	$P = [2,0,1],\ f =$
5	σ_1^-	$f_0{-}1,\ f_1{+}1$	$P = [0,2,1],\ f =$
6	σ_2^-	$f_1{-}1,\ f_2{+}1$	$P = [0,1,2],\ f =$

The final permutation is the identity and the Burau matrix is I_2, confirming this is a topologically trivial braid. Yet the framing is $f = (1,-2,1) \neq (0,0,0)$: residual framed memory survives topological cancellation.

References

[1] F. A. Garside, "The braid group and other groups," *Q. J. Math.* **20**, 235–254 (1969).

[2] J. S. Birman, *Braids, Links, and Mapping Class Groups*, Annals of Mathematics Studies No. 82 (Princeton University Press, 1974).

[3] C. Kassel and V. Turaev, *Braid Groups*, Graduate Texts in Mathematics Vol. 247 (Springer, 2008).

[4] S. O. Bilson-Thompson, "A topological model of composite preons," *arXiv:hep-ph/0503213* (2005).

[5] S. O. Bilson-Thompson, F. Markopoulou, and L. Smolin, "Quantum gravity and the Standard Model," *Class. Quantum Grav.* **24**, 3975–3993 (2007).

[6] P. Dehornoy, with I. Dynnikov, D. Rolfsen, and B. Wiest, *Ordering Braids*, Mathematical Surveys and Monographs Vol. 148 (AMS, 2008).

[7] E. A. El-Rifai and H. R. Morton, "Algorithms for positive braids," *Q. J. Math.* **45**, 479–497 (1994).

[8] Y. Koide, "New viewpoint of quark and lepton mass hierarchy," *Phys. Rev. D* **28**, 252 (1983).

[9] K. Janse van Rensburg, "The Topological Inversion Model: foundations, the Law of Nothing, and Planck-scale reciprocal geometry," in preparation (2026).